THE JOURNAL OF PHYSICAL CHEMISTRY C

Article

pubs.acs.org/JPCC

Constrained Surface Complexation Modeling: Rutile in RbCl, NaCl, and $NaCF_3SO_3$ Media to 250 °C

Michael L. Machesky,*[,†] Milan Předota,[‡] Moira K. Ridley,[§] and David J. Wesolowski[∥]

[†]Illinois State Water Survey, University of Illinois, 2204 Griffith Drive, Champaign, Illinois 61820-7495, United States

[‡]Institute of Physics and Biophysics, Faculty of Science, University of South Bohemia, Branisovska 1760, 370 05 Ceske Budejovice, Czech Republic

[§]Department of Geosciences, Texas Tech University, Lubbock, Texas 79409-1053, United States

[∥]Chemical Sciences Division, Oak Ridge National Laboratory, Oak Ridge, Tennessee 37831-6110, United States

S *Supporting Information*

ABSTRACT: A comprehensive set of molecular-level results, primarily from classical molecular dynamics (CMD) simulations, are used to constrain CD-MUSIC surface complexation model (SCM) parameters describing rutile powder titrations conducted in RbCl, NaCl, and NaTr (Tr = triflate, $CF_3SO_3^-$) electrolyte media from 25 to 250 °C. Rb^+ primarily occupies the innermost tetradentate binding site on the rutile (110) surface at all temperatures (25, 150, 250 °C) and negative charge conditions (−0.1 and −0.2 C/m^2) probed via CMD simulations, reflecting the small hydration energy of this large, monovalent cation. Consequently, variable SCM parameters (Stern-layer capacitance values and intrinsic Rb^+ binding constants) were adjusted relatively easily to satisfactorily match the CMD and titration data. The larger hydration energy of Na^+ results in a more complex inner-sphere distribution, which shifts from bidentate to tetradentate binding with increasing negative charge and temperature, and this distribution was not matched well for both negative charge conditions, which may reflect limitations in the CMD and/or SCM approaches. In particular, the CMD axial density profiles for Rb^+ and Na^+ reveal that peak binding distances shift toward the surface with increasing negative charge, suggesting that the CD-MUSIC framework may be improved by incorporating CD or Stern-layer capacitance values that vary with charge.

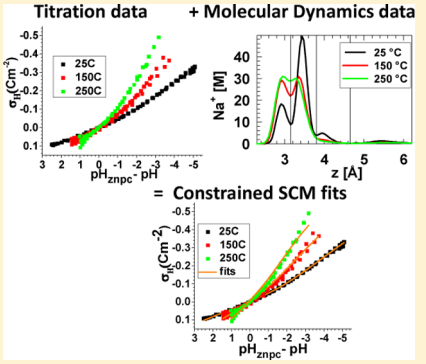

1. INTRODUCTION

In situ spectroscopic and X-ray scattering techniques and computational methods are being used increasingly to precisely reveal the adsorption structures at aqueous mineral−water interfaces.[1] However, these in situ methods are still rather costly, both in time and resources, such that probing a wide range of relevant physiochemical conditions (e.g., pH, solution compositions, and temperature) is difficult. Surface complexation models (SCMs), in which chemical equilibrium expressions describing solution species binding to surface functional groups are modulated by electrostatic effects,[2,3] can fill this niche, given that they are able to make maximum possible use of the molecular level data provided by spectroscopy, scattering, and computation to help constrain model parameters.

Considerable progress has been made in this regard. The first wave of SCMs matured in the 1970s and combined chemical reactions based primarily on solution-phase analogs with electrostatic terms from classical electrical double layer (EDL) theory.[4−7] These models can successfully describe bulk adsorption data, but it was soon realized that a given set of model parameters was not unique. That is, a different yet equally plausible parameter set could describe a given set of adsorption data equally well.[8] Furthermore, the derived parameters were in general found to be invalid outside the narrow range of conditions at which the parameters were determined. Although relevant spectroscopic studies also began to appear in the 1970s, it was not until the mid-1980s that in situ spectroscopic techniques, such as FTIR[9] and synchrotron-based X-ray methods,[10] began to provide the detailed information most useful for constraining SCM parameters. Corresponding computational studies were slower to appear, but by the mid-1990s, computational speed was adequate and available enough for progress to be made.[11,12]

SCMs have also evolved to better utilize molecular scale information. The extended triple layer model (ETLM) of Sverjensky and Fukushi[13] is able to incorporate inner-sphere oxyanion adsorption structures observed spectroscopically. Crystal face specific detail in combination with bond valence theory was used to develop the MUSIC model of surface protonation,[14] which made it possible to estimate and hence constrain relevant intrinsic surface protonation constants within SCMs. Bond valence theory was also incorporated into the charge distribution (CD) concept, whereby adsorbed charge is

Received: March 24, 2015
Revised: May 28, 2015

DOI: 10.1021/acs.jpcc.5b02841
J. Phys. Chem. C XXXX, XXX, XXX−XXX

distributed at the interface according to adsorbate structure.[15] These concepts are combined in the CD-MUSIC model, which represents the current state-of-the art SCM, as it has proven capable of incorporating the widest variety of molecular scale information.[16]

Here, we utilize a comprehensive set of molecular scale information, primarily from classical molecular dynamics (CMD) simulations, that spans a wide range of charge and temperature to help constrain CD-MUSIC model parameters describing rutile titration data collected in RbCl, NaCl, and $NaCF_3SO_3$ [$CF_3SO_3^-$ = triflate (Tr)] electrolyte media from 25 to 250 °C. Although some of these data have been described before with various SCMs, including CD-MUSIC,[17] the present set of CMD and titration data constitute the most compatible and complete sets of molecular and macroscopic information currently available to help constrain SCMs. Consequently, we endeavored to formulate CD-MUSIC SCMs for the RbCl–rutile and combined NaCl–NaTr–rutile systems that are as molecularly consistent as possible. Although a perfect correspondence between the CMD and CD-MUSIC results was not expected, CD-MUSIC was able to incorporate many of the CMD results while also providing good fits to the macroscopic titration data. Moreover, the discrepancies noted suggest CD-MUSIC could be improved by incorporating charge-dependence into the CD or Stern-layer capacitance values.

2. COMPUTATIONAL AND EXPERIMENTAL METHODS

Most of the computational and titration results presented and discussed here were generated with methods that have been described previously. Accordingly, only brief method summaries and relevant literature citations are provided here.

2.1. Classical Molecular Dynamics (CMD) Simulations. We used the same interaction models of the (110) rutile surface, SPC/E water, and ions as in our previous work.[18−21] The relaxed surface structure and flexible surface groups within fixed bond lengths and flexible bond angles with ab initio determined parameters and partial charges described the rutile (110) surface. The interactions among Ti and O surface atoms were found to be properly described by the Matsui and Akaogi potential,[22] and interactions between surface oxygen and aqueous species were described by assigning SPC/E Lennard-Jones parameters to the surface oxygen atoms. The interactions between oxygens of water and Ti atoms were fit to DFT data and then to a Lennard-Jones potential. Lorentz–Berthelot combining rules were used for the interactions between Ti atoms and ions. The cations were either Rb^+ or Na^+, and the anion was Cl^- for all simulations. Our starting surface configuration was the neutral, "nonhydroxylated" (110) surface of rutile wherein water molecules are physisorbed atop each under-coordinated surface Ti atom, and bridging oxygen atoms are unprotonated. Each of the two opposing surfaces constraining the aqueous layer had lateral dimensions of 35.508 × 38.981 Å, and the separation between the two surfaces was about 50–60 Å, adjusted to yield the desired pressure.

The neutral surfaces were fully nonhydroxylated, that is, with water molecules physisorbed atop surface Ti atoms, while the negatively charged surfaces with a surface charge density of −0.104 C/m^2 were prepared by addition of 18 terminal hydroxyls and the −0.208 C/m^2 surfaces were prepared by addition of 36 terminal hydroxyls. The positive +0.104 C/m^2 surfaces were prepared by protonation of 18 bridging oxygens to form bridging hydroxyls. With 144 terminal sites and 144 bridging sites, the surfaces remained predominately non-hydroxylated under these charge conditions. The charged surface species (hydroxylated terminal or protonated bridging sites) were set at the beginning of the simulation according to the desired surface charge density and along with SPC/E water did not undergo any proton-exchange reactions. The partial charges of surface atoms were obtained with the same approach as used in our previous studies of hydroxylated and nonhydroxylated surfaces,[18−21] and the resulting values are given in Table 1. The simulated systems were always charge neutral, with the surface charge compensated by adjusting the numbers of ions in the simulation box as given in Table 2. The bulk concentration of ions in the central region of the slab was approximately 0.3 M, whereas concentrations near the interface were much higher (Figures 1 and 2). Simulations were conducted at 25, 150, and 250 °C with corresponding pressures of 1, 4.76, and 39.8 bar (i.e., ambient pressure at 25 °C and liquid–vapor coexistence pressures at high temperatures). These conditions overlapped those of the experimental rutile powder titrations summarized next.

Table 1. Surface Atoms and Their Charges at the Surface Charge Densities (σ, C/m^2) Used in the CMD Simulations

	charges at various surface charge densities			
atom	σ = −0.208	σ = −0.104	σ = 0	σ = +0.104
surface Ti(V) and Ti(VI)	2.121	2.137	2.196	2.175
terminal hydroxyl O	−0.974	−0.956		
terminal hydroxyl H	0.394	0.412		
unprotonated bridging O	−1.053	−1.037	−1.098	−0.997
protonated bridging O				−0.944
bridging H				0.475

Table 2. Number of Ions in the Simulation Box Necessary To Compensate the Surface Charge Densities (C/m^2) and Surface Charge (e) Used in the CMD Simulations

		no. of ions	
surface charge density (C/m^2)	surface charge to compensate (e)	Rb^+ or Na^+	Cl^-
−0.2	−36	48 (Rb^+)	12 (Rb^+)
		51 (Na^+)	15 (Na^+)
−0.1	−18	30	12
0.0	0	18	18
+0.1	18	12	30

2.2. Rutile Titrations. Two separate batches of TIOXIDE rutile powder were used for the titrations. The N_2–BET surface area of batch 1 rutile was approximately 17 m^2/g, and that of batch 2 was approximately 14 m^2/g. Both batches underwent hydrothermal pretreatment before use[23] and thereafter exhibited indistinguishable point of zero net proton charge values (pH_{znpc}) between 25 and 250 °C. Titrations at 25 °C and some at 50 °C were conducted with a glass-electrode autotitrator system, while some titrations at 50 °C and all titrations at 100, 150, 200, and 250 °C were conducted in stirred hydrogen-electrode concentration cells.[23−25] Briefly, 1–1.5 g samples of rutile powder, dominated by the (110) crystal face, were suspended in 40–50 mL of acidic solutions (pH

DOI: 10.1021/acs.jpcc.5b02841
J. Phys. Chem. C XXXX, XXX, XXX–XXX

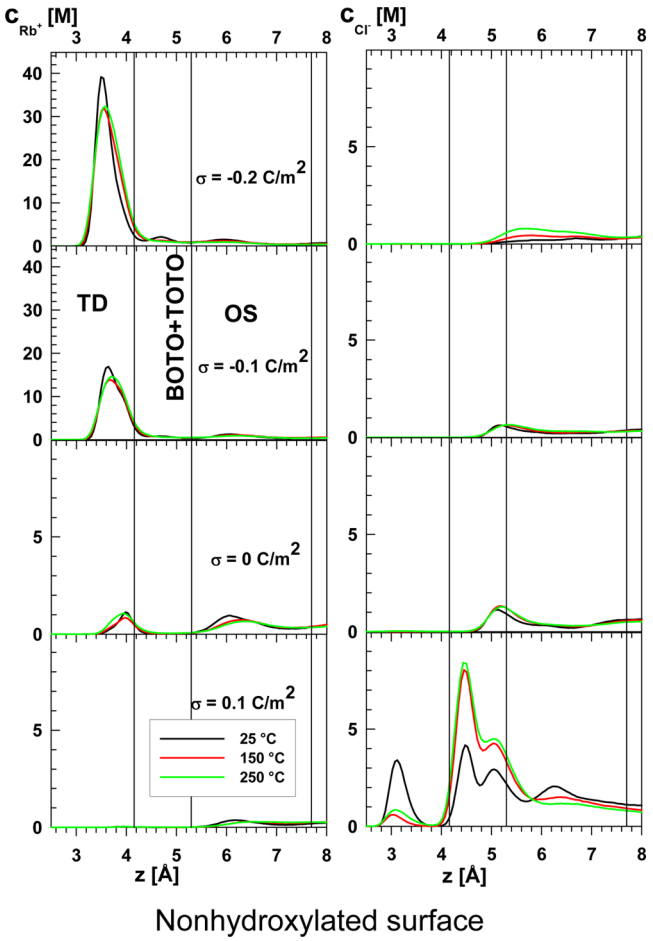

Figure 1. Axial density profiles of Rb^+ (left) and Cl^- (right) for RbCl solutions at the nonhydroxylated rutile (110) surface, as a function of temperature and surface charge density. z (Å) represents the distance above the Ti−O surface plane.

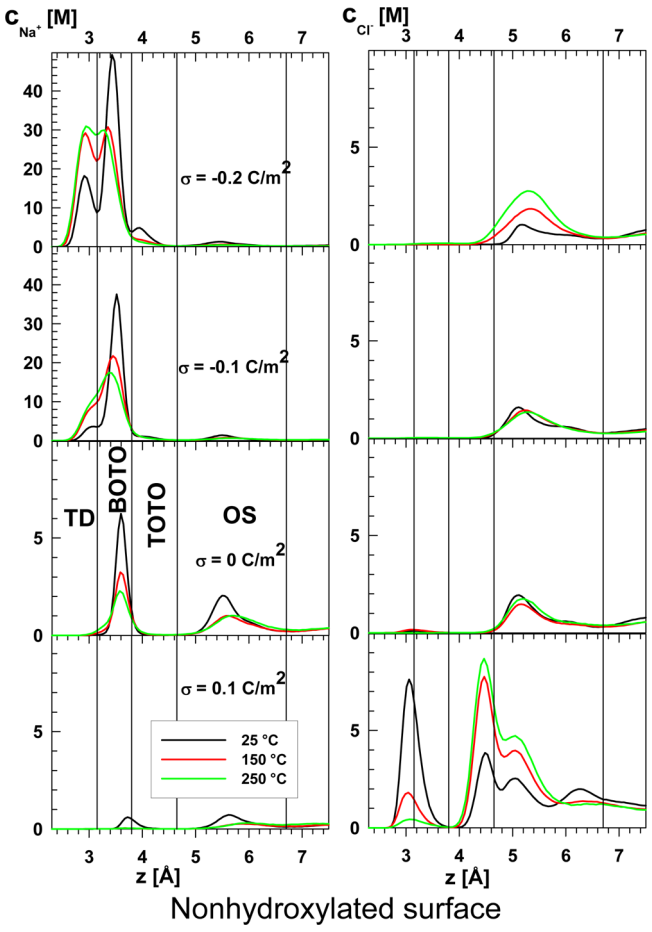

Figure 2. Axial density profiles of Na^+ (left) and Cl^- (right) for NaCl solutions at the nonhydroxylated rutile (110) surface, as a function of temperature and surface charge density. z (Å) represents distance above the Ti−O surface plane.

~2.7) of various but precisely known compositions: (1) 0.03, 0.3, or 1.0 *m* NaCl; (2) 0.03 or 0.3 *m* NaTr; or (3) 0.03 or 0.3 *m* RbCl. Titrations were then conducted at pH 7.5−11 by adding 15−40 aliquots of the base titrant (NaOH or RbOH in the respective electrolyte media). From mass and charge balance considerations, the solution excess or deficit of protons is known at each measured pH value, and this excess or deficit can be expressed in terms of net proton charge per unit surface area of rutile (C/m^2).

2.3. Surface Complexation Modeling. Titration data were fit using Mathematica notebooks. Variable parameters were Stern layer capacitance values (C_S) and ion binding constants (e.g., K_{Cl}), while charge distribution (CD) values were fixed. The CD-MUSIC modeling approach was combined with the basic Stern EDL model following the method of Ridley et al.,[17] but with modifications to account for the CMD simulations presented here. The most significant of those modifications were (1) the use of the nonhydroxylated rather than hydroxylated surface results (rationale provided in section 4.1 below); (2) the use of CMD results to 250 °C rather than only 25 °C; (3) the fixing of CD values and reaction stoichiometry based on the distribution of oxygen atoms (bridging oxygens, terminal oxygens, water molecules) in the first coordination shell of Rb^+, Na^+, and Cl^- as obtained from CMD simulations; and (4) observed CMD Rb^+ and Na^+ site binding ratios (e.g., bidentate/tetradentate) provided numeric targets for SCM fitting.

The ion binding reactions utilized in the SCM were formulated to match the binding configurations observed in the CMD simulations with a few exceptions. First, triflate was the electrolyte anion for some of the titration data (Figure 3, right panels), but the CMD simulations only considered Cl^-. However, NaCl and NaTr titration data conducted at the same temperature and ionic strength were combined and fit together. This was justified because differences between NaCl and NaTr titration data were negligible, at least in part because the titration range over which positive surface charge can develop (below the pH_{znpc}) is relatively limited (approximately, pH 5.4−2.7). Moreover, Tr^- (via the SO_3^- group) may interact with positively charged surface groups similar to Cl^- (section 3.1 below). Second, the CMD observed replacement of some terminal water molecules by Cl^- at positive surface charge (e.g., Figure 2) that was not included in the SCM. These differences are discussed in more detail below.

3. RESULTS

3.1. Classical MD Simulations. The molar ion axial concentration profiles of RbCl solutions above the non-hydroxylated surface of rutile at the −0.2, −0.1, 0, and 0.1 C/m^2 charge states are shown in the left column of Figure 1. Boundaries between cation adsorption sites are indicated by

DOI: 10.1021/acs.jpcc.5b02841
J. Phys. Chem. C XXXX, XXX, XXX−XXX

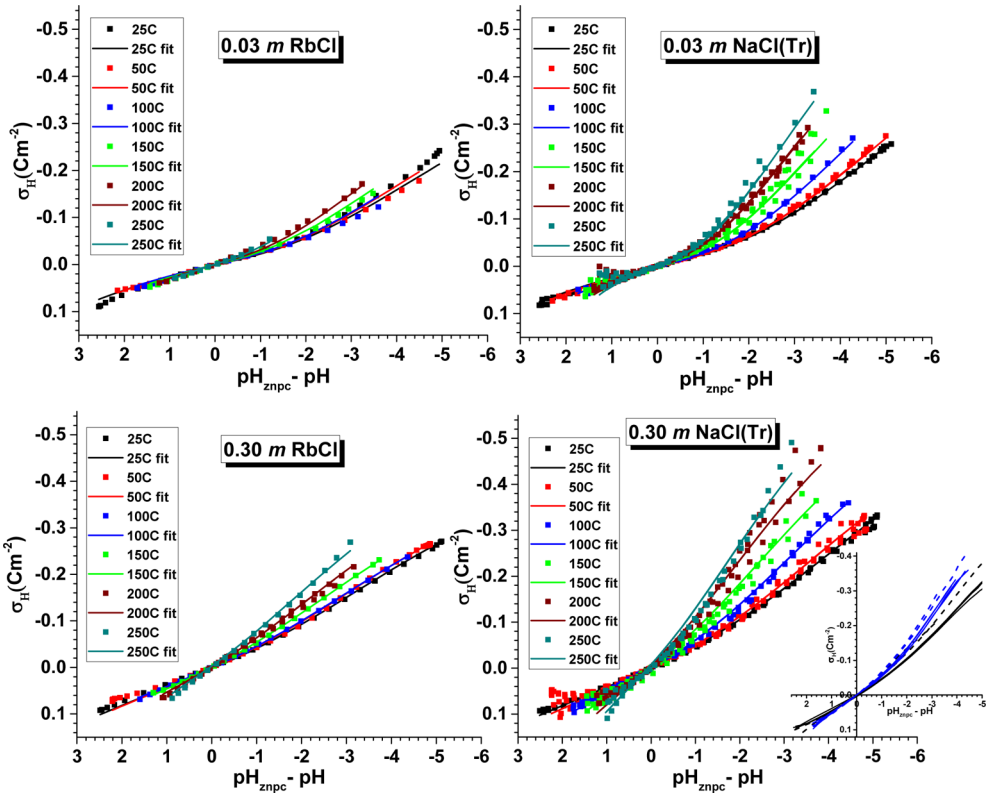

Figure 3. Proton charge (σ_H) vs pH_{znpc} − pH data (solid symbols) and SCM fits (lines) for 0.03 *m* RbCl (upper left) and NaCl(Tr) (upper right) and for 0.30 *m* RbCl (lower left) and NaCl(Tr) (lower right) at 25, 50, 100, 150, 200, and 250 °C. The inset plot in the lower right graph shows σ_H vs pH_{znpc} − pH data for batch 2 rutile (solid lines) and batch 1 rutile (dashed lines) at 25 °C (black) and 100 °C (blue) for 0.30 *m* NaCl(Tr).

vertical lines as identified by local minima in the axial profiles and analysis of lateral density profiles of ions within these boundaries, which unambiguously define the position of adsorbed ions with respect to surface atoms. These boundaries are at 4.16, 5.3, and 7.7 Å above the (110) Ti−O surface plane for the tetradentate/bidentate, bidentate/outer sphere, and outer sphere/bulk solution boundaries, respectively, which are the same as those determined for the hydroxylated surface.[21] Identical boundaries are shown for the Cl^- axial profiles in Figure 1 (right column) only to facilitate comparison with the distribution of Rb^+ (and Na^+ in Figure 2). Those boundaries do not delineate specific Cl^- binding geometries, since those were not determined separately. Note that the concentration of adsorbed Rb^+ is much higher than that of Cl^- on negatively charged surfaces, comparable at neutral surfaces, and lower than that of Cl^- only on the positively charged surface.

Binding is overwhelmingly inner-sphere tetradentate (TD); that is, Rb^+ is bound to two terminal oxygens (TO) and two bridging oxygens (BO) at negative surfaces, with much smaller amounts of inner-sphere bidentate (peak at ca. 4.7 Å) and outer-sphere (OS) Rb^+ (peak at ca. 6 Å) also present. Bidentate Rb^+ binding includes adsorption to two TOs (TOTO) and one TO and one BO (BOTO), with these being difficult to distinguish on the axial density profile because of the large size of Rb^+ and the corresponding Rb−O pair correlation function.[21] Moreover, temperature has minimal effect on Rb^+ distribution at negative surfaces. Small amounts of TD and OS Rb^+ are present on the neutral surface, and adsorbed Rb^+ is barely perceptible at 0.1 C/m^2.

The Cl^- profile at 0.1 C/m^2 is rather complex and temperature-dependent. The innermost peak centered near 3.1 Å represents Cl^- adsorbed in an inner-sphere fashion via exchange with water molecules adsorbed to terminal Ti atoms, and in terms of the SCM detailed below, it can be depicted as follows:

$$Ti{-}OH_2^{0.566+} + Cl^- \rightarrow Ti{-}Cl^{0.434-} + H_2O \quad (1)$$

The peak near 4.5 Å represents Cl^- in contact with the hydrogen of protonated bridging oxygen (BOH) groups, whereas the peak near 5 Å is populated by Cl^- also localized above BOH groups, but not in direct contact with them. Hence, they can be classified as inner- and outer-sphere monodentate, respectively. Finally, a minor outermost peak is also apparent near 6.3 Å at 25 °C and represents Cl^- bound in a nonlocalized, outer-sphere fashion.

MD simulations with triflate as the anion were not conducted. However, the interaction of this anion with the positively charged rutile surface may be similar to that of Cl^-. That is, an oxygen of the negatively charged sulfonate group (SO_3^-) of the triflate anion ($CF_3SO_3^-$) may be in contact with or otherwise be localized above the hydrogen of protonated BOH groups. That the NaCl and NaTr titration curves are indistinguishable in the positive surface charge region would seem to support this hypothesis. Admittedly, however, how the triflate anion actually interacts with the (110) rutile surface awaits molecular scale investigation.

Figure 2 shows the NaCl molar ion axial concentration profiles at the −0.2, −0.1, 0, and 0.1 C/m^2 charge states with the vertical lines representing boundaries between various Na^+ binding sites. These boundaries are at 3.15, 3.80, 4.65, and 6.7 Å for the TD/BOTO, BOTO/TOTO, TOTO/outer sphere, and outer sphere/bulk solution boundaries, respectively.

DOI: 10.1021/acs.jpcc.5b02841
J. Phys. Chem. C XXXX, XXX, XXX−XXX

Table 3. Numbers of Rb^+ and Na^+ Ions Adsorbed as Tetradentate (TD), Bidentate (BOTO and TOTO), and Outer-Sphere (OS) Species for the CMD Charge States Simulated[a]

		−0.2 C/m² (−36 e)					−0.1 C/m² (−18 e)				
ion	temp (°C)	TD	BOTO	TOTO	OS	Cl^-	TD	BOTO	TOTO	OS	Cl^-
Rb^+	25	28.7	2.8		3.4	0.9	14.4	1.5		2.6	1.5
	150	30.2	2.8		3.2	1.5	13.6	1.7		2.8	1.7
	250	32.7	2.8		2.6	2.6	14.5	1.9		2.5	1.9
Na^+	25	10.1	26.5	3.0	2.0	1.7	1.7	18.4	1.0	1.7	2.5
	150	18.9	20.4	1.5	1.2	3.5	4.5	15.5	0.9	1.3	2.6
	250	21.5	19.9	1.1	1.1	5.4	5.4	13.6	1.0	1.3	2.6
		0.0 C/m² (0 e)					+0.1 C/m² (+18 e)				
ion	temp (°C)	TD	BOTO	TOTO	OS	Cl^-	TD	BOTO	TOTO	OS	Cl^-
Rb^+	25	0.64	0.12		1.93	2.34	0.0	0.0		0.9	13.5
	150	0.58	0.15		1.73	2.68	0.0	0.0		0.5	15.7
	250	0.84	0.22		1.62	2.74	0.0	0.0		0.7	16.6
Na^+	25	0.00	2.59	0.14	2.37	2.96	0.0	0.2	0.1	0.9	13.2
	150	0.02	1.60	0.19	1.53	2.52	0.0	0.0	0.0	0.5	14.0
	250	0.06	1.99	0.28	1.42	3.10	0.0	0.0	0.0	0.6	15.4

[a]The Cl^- column contains the total number of atoms within the outer-sphere boundary, irrespective of binding state.

Boundaries on the hydroxylated surface were slightly different, 3.13, 3.50. 4.75, and 7.0 Å, respectively.[21] Unlike for Rb^+, the bidentate BOTO and TOTO configurations can be distinguished by peaks at ca. 3.4 and 3.9 Å, respectively. In addition, the Na^+ profiles show a much more complex charge and temperature dependence than those for Rb^+. Inner-sphere TD, BOTO, and TOTO species are all present at both negative charge conditions, with BOTO the dominant bidentate complex and the TD complex increasing with both negative charge and temperature. Similar trends also occur on the negative hydroxylated surface, where, however, the dominant bidentate complex is TOTO under ambient conditions and for −0.1 C/m² charge, even at elevated temperatures.[21] The interfacial distribution of Cl^- is similar to that observed for RbCl.

The numbers of Rb^+ and Na^+ ions adsorbed at the binding sites identified for all modeled charge states and temperatures are given in Table 3, along with the total number of Cl^- ions within the outer-sphere boundary, irrespective of binding state. These data, or more specifically ratios between dominant adsorption sites (e.g., BOTO/TD for Na^+), were used to help constrain the SCM results presented and discussed below. We also calculated the average numbers of BO's, TO's, and oxygens of water molecules in the first solvation shells of Rb^+ and Na^+ in the various adsorption geometries and in the bulk at the −0.2, −0.1, and 0 C/m² charge states and for Cl^- in the 0.1 C/m² charge state. Oxygen atoms were counted up to the minimum after the first peak of the $g_{\text{cation-O}}$ radial distribution functions, which were 3.81, 3.26, and 3.86 Å for Rb^+−O, Na^+−O, and Cl^-−O, respectively, for all oxygens, temperatures, and charge states. These numbers were used to determine adsorption reaction stoichiometry (Table 4) and to fix the charge distribution (CD) values (Table 5) associated with the SCM.

3.2. Rutile Titrations. Titration results and SCM fits at all temperatures are given in Figure 3 for RbCl media (left) and NaCl(Tr) media (representing combined NaCl and NaTr media titrations) (right). The NaCl and NaTr data for batch 2 rutile were combined, since titration curves were indistinguishable at each temperature and ionic strength (0.03 and 0.30 *m*) investigated. The results are presented relative to the pH of zero net proton charge (pH_{znpc} − pH) at each temperature,

Table 4. Surface Complexation Reactions Considered and Corresponding Equilibrium Constant Designations[a]

complexation reactions	equil const
surface protonation	
$\equiv TiOH^{0.434-} + H^+ \rightarrow \equiv TiOH_2^{0.566+}$	K_{H1}
$\equiv Ti_2O^{0.555-} + H^+ \rightarrow \equiv Ti_2OH^{0.445+}$	K_{H2}
inner-sphere Rb^+	
$2\equiv TiOH^{0.434-} + 2\equiv Ti_2O^{0.555-} + Rb^+ + vH^+ \rightarrow [(\equiv(2-v)TiOH^{0.434-})(\equiv vTiOH_2^{0.566+})(\equiv Ti_2O^{0.555-})_2]-Rb^+$	K_{Rb} (TD)
$\equiv TiOH^{0.434-} + \equiv Ti_2O^{0.555-} + Rb^+ + wH^+ \rightarrow [(\equiv(1-w)TiOH^{0.434-})(\equiv wTiOH_2^{0.566+})(\equiv Ti_2O^{0.555-})]-Rb^+$	K_{Rb} (BOTO)
outer-sphere Rb^+	
$\equiv TiOH^{0.434-} + Rb^+ \rightarrow (\equiv TiOH^{0.434-})-Rb^+$	K_{Rb} (OS)
$\equiv Ti_2O^{0.555-} + Rb^+ \rightarrow (\equiv Ti_2O^{0.555-})-Rb^+$	K_{Rb} (OS)
inner-sphere Na^+	
$2\equiv TiOH^{0.434-} + 2\equiv Ti_2O^{0.555-} + Na^+ + xH^+ \rightarrow [(\equiv(2-x)TiOH^{0.434-})(\equiv xTiOH_2^{0.566+})(\equiv Ti_2O^{0.555-})_2]-Na^+$	K_{Na} (TD)
$\equiv TiOH^{0.434-} + \equiv Ti_2O^{0.555-} + Na^+ + yH^+ \rightarrow [(\equiv(1-y)TiOH^{0.434-})(\equiv yTiOH_2^{0.566+})(\equiv Ti_2O^{0.555-})]-Na^+$	K_{Na} (BOTO)
$2\equiv TiOH^{0.434-} + Na^+ + zH^+ \rightarrow [(\equiv(2-z)TiOH^{0.434-})(\equiv zTiOH_2^{0.566+})]-Na^+$	K_{Na} (TOTO)
outer-sphere Na^+	
$\equiv TiOH^{0.434-} + Na^+ \rightarrow (\equiv TiOH^{0.434-})-Na^+$	K_{Na} (OS)
$\equiv Ti_2O^{0.555-} + Na^+ \rightarrow (\equiv Ti_2O^{0.555-})-Na^+$	K_{Na} (OS)
inner-sphere BOH Cl^- (and Tr^-)	
$\equiv Ti_2O^{0.555-} + H^+ + Cl^- \rightarrow (\equiv Ti_2OH^{0.445+})-Cl^-$	K_{Cl} (BOH)

[a]The variables *v*, *w*, *x*, *y*, and *z* represent the number of $TiOH_2^{0.566+}$ groups participating in the various inner-sphere Rb^+ and Na^+ complexes modeled as given in Table 5.

which clearly highlights surface charge differences with respect to both temperature and ionic medium. The NaCl(Tr) titration data also revealed that the batch 1 curves were noticeably steeper than batch 2 curves above the pH_{zpnc} at 25, 50, and 100 °C, while differences were negligible at 150, 200, and 250 °C. The inset in the lower right panel of Figure 3 presents these differences at 25 and 100 °C for 0.30 *m* NaCl. It is apparent that the batch 1 surface charge data (dashed lines) are steeper than the batch 2 results (solid lines) under negative charge conditions (pH_{znpc} − pH < 0) and that the difference is greater at 25 °C than at 100 °C. The specific reasons for these

DOI: 10.1021/acs.jpcc.5b02841
J. Phys. Chem. C XXXX, XXX, XXX−XXX

Table 5. Basic Stern CD-MUSIC Model Parameters for RbCl (top panel), NaCl(Tr) (middle panel), and NaCl (bottom panel) Media[a]

Batch 2

					TD				BOTO				OS	BOH		
temp (°C), salt	$\log K_{H1}$ [b]	$\log K_{H2}$ [b]	pH_{znpc} [b]	C_S (F/m^2)	$\log K_{Rb}$	O_{tot}	v TiOH	CD	$\log K_{Rb}$	O_{tot}	w $TiOH_2$	CD	$\log K_{Rb}$	$\log K_{Cl}$	CD	MSC
25, RbCl	5.94	4.89	5.42	0.64	−1.00	8.25	1.70	0.48	−1.80	8.25	0.85	0.24	−1.10	−0.05	−0.14	4.57
50, RbCl	5.61	4.61	5.12	0.60	−0.90	8.20	1.70	0.49	−1.75	8.20	0.85	0.24	−1.10	−0.05	−0.14	4.88
100, RbCl	5.12	4.21	4.68	0.49	−0.75	8.09	1.70	0.49	−1.70	8.09	0.85	0.25	−1.10	−0.05	−0.14	4.78
150, RbCl	4.83	3.97	4.41	0.51	−0.60	7.98	1.70	0.50	−1.65	7.98	0.85	0.25	−1.10	−0.05	−0.14	5.52
200, RbCl	4.63	3.81	4.23	0.56	−0.50	7.87	1.70	0.51	−1.65	7.87	0.85	0.25	−1.10	−0.05	−0.14	5.02
250, RbCl	4.50	3.70	4.11	0.67	−0.35	7.76	1.70	0.52	−1.65	7.76	0.85	0.26	−1.10	−0.05	−0.14	5.05

Batch 2 only for 25, 50, and 100 °C; Combined Batches 1 and 2 for 150, 200, and 250 °C

		TD				BOTO				TOTO				OS	BOH		
temp (°C), salt	C_S (F/m^2)	$\log K_{Na}$	O_{tot}	x $TiOH_2$	CD	$\log K_{Na}$	O_{tot}	y $TiOH_2$	CD	$\log K_{Na}$	O_{tot}	z $TiOH_2$	CD	$\log K_{Na}$	$\log K_{Cl,Tr}$	CD	MSC
25, NaCl(Tr)	0.64	−1.55	6.76	1.30	0.59	−0.85	6.08	0.50	0.33	−1.45	6.09	1.40	0.33	−1.20	−0.05	−0.14	6.41
50, NaCl(Tr)	0.64	−1.40	6.70	1.30	0.60	−0.90	6.05	0.50	0.33	−1.50	6.07	1.40	0.33	−1.30	−0.05	−0.14	4.16
100, NaCl(Tr)	0.70	−1.10	6.59	1.20	0.61	−0.85	5.99	0.40	0.33	−1.60	6.00	1.40	0.33	−1.60	−0.05	−0.14	5.97
150, NaCl(Tr)	0.77	−0.65	6.48	1.20	0.62	−0.70	5.93	0.40	0.34	−1.65	5.96	1.40	0.34	−1.75	−0.05	−0.14	3.99
200, NaCl(Tr)	0.98	−0.35	6.37	1.20	0.63	−0.65	5.88	0.40	0.34	−1.80	5.86	1.40	0.34	−1.80	−0.05	−0.14	3.96
250, NaCl(Tr)	1.20	−0.20	6.26	1.20	0.64	−0.60	5.82	0.35	0.34	−1.70	5.78	1.40	0.34	−1.90	−0.05	−0.14	3.84

Batch 1

		TD				BOTO				TOTO				OS	BOH		
temp (°C), salt	C_S (F/m^2)	$\log K_{Na}$	O_{tot}	x $TiOH_2$	CD	$\log K_{Na}$	O_{tot}	y $TiOH_2$	CD	$\log K_{Na}$	O_{tot}	z $TiOH_2$	CD	$\log K_{Na}$	$\log K_{Cl}$	CD	MSC
25, NaCl	0.82	−1.55	6.76	1.30	0.59	−0.85	6.08	0.50	0.33	−1.45	6.09	1.40	0.33	−1.20	−0.05	−0.14	5.19
50, NaCl	0.82	−1.40	6.70	1.30	0.60	−0.90	6.05	0.50	0.33	−1.50	6.07	1.40	0.33	−1.30	−0.05	−0.14	4.72
100, NaCl	0.83	−1.10	6.59	1.20	0.61	−0.85	5.99	0.40	0.33	−1.60	6.00	1.40	0.33	−1.60	−0.05	−0.14	5.27
150, NaCl	0.85	−0.65	6.48	1.20	0.62	−0.70	5.93	0.40	0.34	−1.65	5.96	1.40	0.34	−1.75	−0.05	−0.14	4.38
200, NaCl	0.93	−0.35	6.37	1.20	0.63	−0.65	5.88	0.40	0.34	−1.80	5.86	1.40	0.34	−1.80	−0.05	−0.14	4.04
250, NaCl	1.35	−0.20	6.26	1.20	0.64	−0.60	5.82	0.35	0.34	−1.70	5.78	1.40	0.34	−1.90	−0.05	−0.14	3.66

[a]The intrinsic equilibrium constants (log K) correspond to the reactions given in Table 4. C_S is the Stern-layer capacitance value, O_{tot} is the total number of oxygen atoms in the primary coordination sphere of Rb^+ or Na^+ adsorbed as (left to right) TD, BOTO, and TOTO (Na^+ only) complexes, and v, w, x, y, and z represent the corresponding number of oxygens as $TiOH_2^+$ groups. CD values represent those portions of Rb^+, Na^+, or Cl^- and Tr^- charge attributed to the surface plane (remaining charge at the Stern plane), and the model selection criterion (MSC) values are a goodness of fit measure (larger is better). [b]From Machesky et al.[28]

DOI: 10.1021/acs.jpcc.5b02841
J. Phys. Chem. C XXXX, XXX, XXX−XXX

differences are not known, although temperature may have played a role, since the batch 1 and 2 curves coalesced at 150 °C and above. It is also possible that factors such as particle morphology, surface roughness, or other defects could have contributed to the differences. Bourikas et al.[26] divided the room temperature charging data for titanium oxides into those with higher (1.6 C/m^2) and lower (0.9 C/m^2) Stern-layer capacitance values and suggested that the difference was due to surface roughness, with the lower capacitance group being more well-crystallized. Livi et al.[27] characterized the atomic scale edge morphology of the same batch 2 rutile used in this study with detailed STEM HAADF imaging and estimated that one-third of the predominant (110) faces may be populated by steps at the atomic scale. Although batch 1 rutile was not similarly characterized, it is conceivable that its step population or other imperfections could be significantly different from those of batch 2 rutile and affect charging behavior. It is also possible that the batch differences become less apparent above 100 °C, because surface imperfections are somehow smoothed at the relatively acidic conditions (pH ∼2.7) from which the rutile titrations commenced after an overnight equilibration period.[25] In any case, the 25, 50, and 100 °C NaCl(Tr) data presented in Figure 3 are for batch 2 rutile, while combined batch 2 and batch 1 data are presented at 150, 200, and 250 °C. The experimental data and SCM model fits for Figure 3 and for all additional experimental conditions are provided in the Supporting Information.

3.3. Surface Complexation Modeling. The ion binding reactions used are given in Table 4. Note that the fractional charges for the TO and BO groups, as well as their protonation reactions and corresponding equilibrium constants, come directly from earlier work.[28] However, all other reactions in Table 4 have not been used before and were formulated to closely match observed CMD binding configurations. Specifically, the configurations that involve TO groups in inner-sphere Rb^+ and Na^+ binding (e.g., TD, BOTO, and TOTO) explicitly incorporate the number of those TO groups existing as TOH_2 in the adsorption complex. Those quantities are represented by the variables, v, w, x, y, and z, in Table 4 and represent the number of TOH_2 groups participating in TD Rb^+, bidentate (TOBO+TOTO) Rb^+, TD Na^+, BOTO Na^+, and TOTO Na^+ adsorption complexes, respectively. Table 5 contains the numerical values for these variables as determined from the CMD simulations. The number of TOH groups participating in the various adsorption complexes are then fixed by difference as, for example, $2 - v$ for TD Rb^+ and $1 - y$ for BOTO Na^+. Additionally, all Cl^- binding is represented solely by the observed inner-sphere association with BOH groups (section 3.1).

The SCM fitting process was as follows. The numbers of Rb^+ and Na^+ ions in specific binding configurations (Table 3) were used to calculate binding site ratios at each negative and neutral charge condition and temperature (e.g., BOTO/TD), which were then matched as closely as possible by adjustment (both freely optimized and manual) of the corresponding Stern-layer capacitance values and intrinsic binding constants. Corresponding CD values were fixed at values predicted from the CMD simulations. These CD values were fixed on the basis of the inner-sphere binding configurations observed (TD = 4, BOTO +TOTO = 2), divided by the total number of oxygen atoms in first coordination sphere of Rb^+ and Na^+ (the O_{tot} values in Table 5). The CD value for Cl^- in inner-sphere monodentate coordination with BOH was determined similarly. The total number of water molecules and BOH groups within the primary coordination sphere of adsorbed Cl^- at 25, 150, and 250 °C was 7.36, 6.98, and 6.73, respectively. Given this small decrease in adsorbed Cl^- hydration, which translates into a 0.01 difference in calculated CD values, it was decided to fix the CD value for Cl^- (and Tr^-) at the temperature-averaged CD value (CD = z/n = −1/7.03 = −0.14) for all SCM simulations.

Model parameters are given in Table 5 for rutile in RbCl media (top), NaCl(Tr) media (middle), and NaCl media (bottom). All RbCl titrations utilized batch 2 rutile and all NaCl-only titrations (bottom panel) utilized batch 1 rutile. The NaCl(Tr) parameters given in the middle panel represent only batch 2 rutile at lower temperatures (25, 50, 100 °C) and combined batch 1 and batch 2 rutile at higher temperatures (150, 200, 250 °C), since the surface charge curves at both 0.03 and 0.30 m were virtually indistinguishable. The protonation constant (log K_{H1} and log K_{H2}) and pH of zero net proton charge (pH_{znpc}) values are from previous studies,[23,28] while the Stern-layer capacitance values (C_S), as well as the remaining log K and model selection criterion (MSC) values, were determined in this study.

4. DISCUSSION

4.1. Nonhydroxylated vs Hydroxylated CMD Results. Our CMD simulations employ nondissociable SPC/E water molecules, and hence, bulk or surface proton exchange reactions are not possible during simulation. Consequently, the charge state of the surface must be set manually beforehand, starting from either the neutral hydroxylated or neutral nonhydroxylated surface. On the neutral hydroxylated surface, hydroxyl groups terminate 5-fold coordinated Ti atoms (Ti−OH) and each BO atom is protonated (BOH), while the neutral nonhydroxylated surface is populated by bare BO atoms and water molecules terminate the 5-fold coordinated Ti atoms ($Ti-OH_2$). In alternate terminology, water is "associated" on the nonhydroxylated surface and "dissociated" on the hydroxylated surface. Charge is generated on the hydroxylated surface by either removing protons from BOH groups to create negative charge or adding protons to Ti−OH groups to create positive charge, while protons are removed from $Ti-OH_2$ groups or added to BO groups to generate negative or positive nonhydroxylated surfaces, respectively.

These differences impact our SCM efforts because hydroxylated and nonhydroxylated surfaces bind ions somewhat differently. This was first noted by Předota and Vlcek,[20] and a more specific comparison can be made between the nonhydroxylated results of the present study and the hydroxylated surface results reported by Předota et al.,[21] which concern the same ions, surface charge states, and temperatures. Boundaries between the various binding configurations, particularly for Na^+, are a bit different between the hydroxylated and nonhydroxylated simulations (see section 3.1). Nevertheless, ion-binding trends for both surfaces are similar, most notably in that under negative charge conditions TD binding of Rb^+ is always dominant and becomes more so for Na^+ with increasing negative charge and temperature. The most significant difference concerns bidentate binding, where BOTO binding tends to dominate at nonhydroxylated surfaces and TOTO binding at hydroxylated surfaces. This difference is understandable given that BOs are unprotonated at nonhydroxylated surfaces and TOs usually contain one proton (rather than two) at hydroxylated surfaces. There is also more inner-sphere binding of Na^+ (as TOTO) at neutral

DOI: 10.1021/acs.jpcc.5b02841
J. Phys. Chem. C XXXX, XXX, XXX−XXX

hydroxylated surfaces than at neutral nonhydroxylated ones. Chloride binding at +0.1 C/m^2 charge is also similar at both surfaces, but with somewhat greater replacement of terminal water molecules (eq 1) at the nonhydroxylated surface because associated water molecules occupy all terminal sites on the positive nonhydroxylated surface but only one-eighth of these sites on the positive hydroxylated surface.

In our MUSIC model surface protonation scheme,[28] the protonation constant of BO is less than that of Ti−OH ($K_{H2} < K_{H1}$ in Table 5), meaning that the more acidic BO will be the dominant negatively charged site, and conversely, Ti−OH_2 will be the dominant positively charged site. At 25 °C and the pH_{znpc} (5.4) about 77% of the rutile (110) surface groups exist as BO and Ti−OH_2 combined. As these are also the dominant site types on the nonhydroxylated surface, our SCM modeling efforts focused on matching the CMD results for that surface. Moreover, there is other molecular-level support for the dominance of BO and Ti−OH_2 on the neutral rutile (110) surface. Kumar et al.[29] found that water was 25% dissociated (corresponding to 75% Ti−OH_2 + BO surface groups) on the rutile (110) surface from DFTMD simulations, although in a later study they cautioned that DFT alone was unable to definitively distinguish between partially dissociated and fully associated water because of the small energy differences involved.[30] Raju et al.[31] predicted water to be 23% dissociated on the rutile (110) surface from MD simulations with the REAXFF force field, while Huang et al.[32] observed 10% dissociated water also via REAXFF MD simulations. Titanium−oxygen distances are longer for Ti−OH_2 than for Ti−OH, with the plane wave DFT calculations of Bandura et al.[33] providing distance ranges of 2.20−2.30 Å for the former and 1.88−2.00 Å for the latter. Given this difference, Zhang et al.[34] were able to estimate from X-ray crystal truncation rod measurements in DI water (pH 5.6) that the observed Ti−O distance of 2.13 Å corresponded to 30(±15)% dissociated water. The Ti−O distance decreased to 2.05 Å at pH 12 in the presence of 1 *m* RbCl, from which they estimated that dissociated water had increased to 65(±15)%. In comparison, our MUSIC model surface protonation scheme predicts water is about 84% dissociated under those solution conditions.

4.2. SCM Parameter Trends. SCM fits to the RbCl and NaCl(Tr) titration data are generally good, as can be seen in Figure 3, as well as in the data tabulated in the Supporting Information. The MSC values in Table 5 quantify the goodness of fit and range from 3.6 to 6.5. Various other modeling schemes have also been used to fit some of these titration data, and similar or even higher MSC values have resulted.[17,28] However, the present SCM results are constrained more fully by the available molecular level information, particularly over a wide range of temperatures and surface charge states.

The present SCM is based on that developed by Ridley et al.,[17] and consequently, modeled reactions are similar, consisting of inner-sphere tetradentate and bidentate adsorption, as well as outer-sphere binding. Moreover, some of the same titration data were fit by Ridley et al.,[17] specifically those for batch 2 rutile in both RbCl and NaCl media at 25 and 50 °C. Consequently, it was possible to fix the batch 2 Stern-layer capacitance values (C_S) to those determined by Ridley et al.[17] at 25 °C (0.64 C/m^2), whereas batch 1 C_S values are greater (0.82 C/m^2), reflecting the greater degree of negative surface charge development. At higher temperatures, batch 1 and batch 2 C_S values in NaCl and NaCl(Tr) media increase, reflecting increasing negative surface charge development, while C_S values for RbCl are lower at 50, 100, 150, and 200 °C than at 25 °C. This decrease in capacitance values is attributable to the relatively slight enhancement in negative surface charge development between 25 and 200 °C (Figure 3, left) being more than offset by the effect of the temperature increase on the SCM electrostatic terms, which are simulated with the C_S and CD parameters. That is, model-derived surface potentials increase with temperature, for example, from 55 mV/pH unit at 25 °C to 88 mV/pH unit at 200 °C, which is similar to the increase in the Nernst potential slope over the same temperature range (59−94 mV/pH unit). Consequently, given that CD values were held at CMD-derived values, C_S values needed to decrease to moderate the increased potentials.

As temperature increases, negative surface charge development increases much more sharply in NaCl(Tr) than RbCl media, reflecting the movement of more Na^+ to the innermost TD binding site (Figure 2), whereas TD binding always predominates for Rb^+ under negative charge conditions (Figure 1). Consequently, the intrinsic Na^+ TD binding constant increases more between 25 and 250 °C (log *K* from −1.55 to −0.20) than does the Rb^+ TD constant (from −1.00 to −0.35). The remaining binding constants for both Rb^+ and Na^+ are less temperature dependent. The bidentate BOTO constants for both Rb^+ and Na^+ increase slightly between 25 and 250 °C, while the Na^+ TOTO constant and Na^+ OS constant decrease slightly, again reflective of both Rb^+ and Na^+ moving closer to the surface with increasing temperature as BOTO and ultimately TD adsorption complexes. In our previous SCMs utilizing the batch 1 NaCl data,[23,35,36] we considered Na^+ binding to be dominated by one complex over the entire range of pH and temperature, which the CMD results demonstrate is too simple a picture.

The decreased degree of cation hydration with increasing temperature is also reflected in the CMD-derived CD values for TD binding, which increase slightly (≤0.05 valence units) with temperature. For example, the total number of oxygen atoms in the first coordination sphere of Na^+ adsorbed in TD fashion at −0.2 C/m^2 charge are 6.76 at 25 °C and 6.26 at 250 °C (Table 5), which results in CD values of 0.59 (4/6.76) and 0.64 (4/6.26), respectively. The CMD-derived bulk solution primary hydration numbers for Rb^+ and Na^+ also decrease with increasing temperature, consistent with previous studies.[37,38]

Some of the CMD results for Cl^- binding were also incorporated into the SCM, even though Cl^- binding trends with respect to charge could not be established because of the narrow pH window experimentally available. Nevertheless, given that CMD axial density profiles for Cl^- were very similar in both RbCl and NaCl media, as expected, the corresponding SCM parameters were constrained to be equal for the single inner-sphere monodentate complex considered.

4.3. Binding Site Ratio Agreement. The site occupancies given in Table 3 were used to calculate binding site ratios (e.g., BOTO/TD) for Na^+ at the −0.2, −0.1, and 0 C/m^2 charge states to provide numeric targets for SCM fitting. Despite numerous attempts, it was not possible to match any single ratio at all charge states for any temperature closely. Consequently, the −0.2 C/m^2 charge state and the ratios between the predominant inner-sphere Rb^+ and Na^+ adsorption configurations at that charge state, (BOTO + TOTO)/TD and BOTO/TD, respectively, were chosen as the primary numeric targets. SCM parameters (Stern-layer capacitance values and relevant binding constants) were adjusted (typically free optimization followed by manual adjustment) to best match

DOI: 10.1021/acs.jpcc.5b02841
J. Phys. Chem. C XXXX, XXX, XXX−XXX

the CMD ratios using the 0.3 *m* ionic strength experimental data (nearest the effective ionic strength of the CMD simulations), while also attaining a reasonable fit to all experimental data.

The MD and fitted SCM ratios for Rb^+ are given in Figure 4 (top). Rb^+ (BOTO + TOTO)/TD ratios are always <0.30

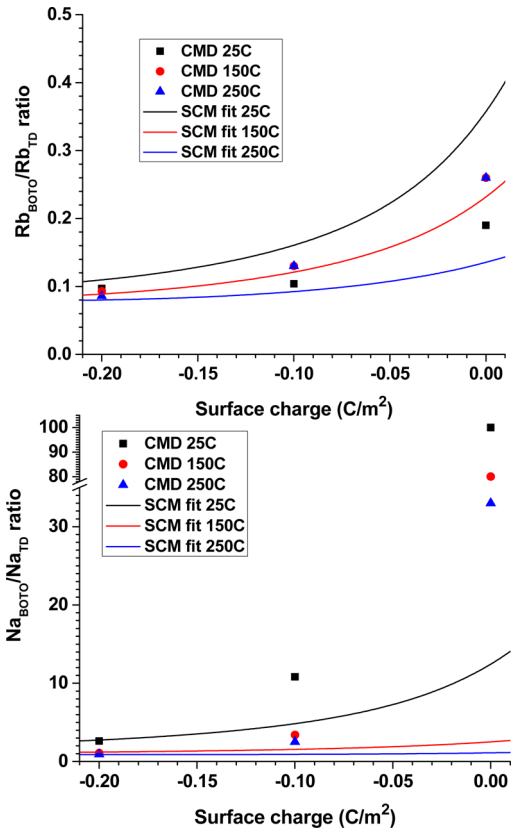

Figure 4. Bidentate/tetradentate binding site ratios from CMD simulations at −0.2, −0.1, and 0 C/m^2 surface charge and 25, 150, and 250 °C (symbols) and corresponding SCM fit ratios (lines) for RbCl (top) and NaCl(Tr) (bottom). Note the *y*-axis break in the lower graph. The NaCl(Tr) MD ratio at 25 °C and 0 surface charge (100) is an estimate.

because of the dominance of the TD complex. Consequently, closely matching the −0.2 C/m^2 ratios also resulted in reasonable agreement at −0.1 and even 0 C/m^2, even though only fractions of Rb^+ atoms contribute to the ratio at the latter charge condition (e.g., 0.15/0.58 at 150 °C).

The Na^+ BOTO/TD ratios (Figure 4, bottom) decrease with increasing temperature because of the increasing dominance of TD binding. Ratios vary more widely than those for Rb^+, ranging from 1 to 100 (with 100 a rough estimate because no Na^+ was bound in TD fashion at 0 C/m^2 and 25 °C). After adjusting the TD and BOTO binding constants to closely match the BOTO/TD ratios at −0.2 C/m^2, the ratios at −0.1 and 0 C/m^2 were significantly underpredicted. This mismatch also extended to other ratios, in particular to those between BOTO and TOTO for all charge conditions. Despite these discrepancies, only small adjustments to the intrinsic binding constants were necessary to better match binding site ratios at −0.1 rather than −0.2 C/m^2. For example, the 250 °C BOTO/TD ratio for Na^+ at −0.1 C/m^2 (2.5) is nicely matched by decreasing the TD binding constant 0.2 log units and increasing the BOTO binding constant 0.2 log units from those values providing a close match at −0.2 C/m^2 (−0.20 and −0.60, respectively, Table 5).

Limitations in both the CMD and SCM approaches are likely responsible for the inability to better match all Rb^+ and Na^+ ratios simultaneously. The CMD model employs nondissociable SPC/E water, which requires the modeled surface charge states to be set manually.[19] Moreover, our basic Stern SCM is composed of two smooth planes of charge (one representing the surface and the second the oppositely charged Stern plane), and electrostatic potentials are governed by continuum electrostatics, both of which are rather crude approximations at the molecular level. One manifestation of continuum electrostatics, as embodied in the Gouy−Chapmann−Stern theory, is apparent in Figure 4, where, as temperature increases, the predicted site ratios increase more slowly between −0.2 and 0 C/m^2 charge. This follows directly from temperature appearing in the denominator of the Boltzmann factor, $\exp(-F\Psi/RT)$, used to correct intrinsic binding constants (Table 5) for model-derived interfacial potentials (Ψ). For example, between 0 and −0.2 C/m^2 surface charge the Rb^+ BOTO binding constant increases from −1.80 to 1.87 log units at 25 °C but only from −1.65 to 0.63 log units at 250 °C. Finally, the CMD simulations apply strictly to the (110) surface of rutile with a given distribution of charged sites, while the titrations were performed on two distinct batches of rutile powder containing other crystal planes as well as various defects along with the dominant (110) surface (see section 3.2 above). Nevertheless, the present CMD and titration data, spanning a wide range of charge and temperature, constitute the most compatible and complete sets of molecular and macroscopic information currently available to help constrain SCMs.

4.4. SCM Agreement with Other Molecular Scale Information. Several other types of molecular scale information exist with which to help gauge the accuracy of the SCM approach, at least near room temperature. That the nonhydroxylated surface better agrees with our surface protonation scheme, as well as with computational and experimental evidence that water is partially dissociated on the neutral (110) surface, is discussed in section 4.1. Additionally, the X-ray crystal truncation study of Zhang et al.[34] determined that the monolayer surface coverage of tetrahedrally coordinated Rb^+ (1 ML = 1 Rb^+ per 19.24 $Å^2$) was 0.4 ± 0.1 ML in 1 *m* RbCl at pH 12. Although these solution conditions are beyond those directly included in the SCM, extrapolation to those conditions results in a very similar surface coverage of 0.38 ML. In a related study, Kohli et al.[39] used resonant anomalous X-ray reflectivity (RAXR) to interrogate the vertical density profile of Rb^+ in 1 mM RbOH solution at pH 11 above the rutile (110) surface. Extrapolating the SCM to those solution conditions results in 0.12 ML coverage, which compares less favorably with that measured (0.080 ± 0.003 ML). Additionally, the root-mean-square width of the RAXR data (0 ± 0.2 Å) is consistent with the multisite nature of the CMD (and SCM) results. That is, mostly tetradentate binding but also some bidentate Rb^+ binding.

There is also some molecular level support for the fitted (C_S) values at 25 °C, which is the primary SCM fitting parameter governing interfacial electrostatics. Parez et al.[40] investigated the dielectric properties of water above the rutile (110) surface at 25 °C with nonequilibrium CMD simulations. CMD-derived C_S values depend sensitively on the location of the surface

DOI: 10.1021/acs.jpcc.5b02841
J. Phys. Chem. C XXXX, XXX, XXX−XXX

charge plane. The height of the surface charge plane needed to agree with the fit SCM values (0.6−0.8 F/m^2) is about 1.7 Å above the first layer of coplanar Ti−O atoms on the (110) surface, which is between the heights of the charge-bearing BO (∼1.2 Å) and TO (∼2.0 Å) groups. Thus, the position of the surface charge plane is fully consistent with BO and TO oxygens as the charge-defining species on rutile (110). It was also concluded that the electrostatic potential profile above the rutile (110) surface was dominated by water, with the dissolved salts (0.35 M NaCl) being only of minor influence. Cheng and Sprik[41] employed DFTMD to calculate C_S at the aqueous rutile (110) surface. Two different calculation methods resulted in virtually identical C_S values of ∼0.4 F/m^2, which is within a factor of 2 of the SCM estimates of this study and those of Ridley et al.[17]

4.5. CMD Binding Features Not Incorporated into the SCM. The CMD simulations revealed several binding features that were not explicitly incorporated into the SCM. The replacement of terminal water molecules by Cl^- at positively charged (+0.1 C/m^2) surfaces (Figures 1 and 2) as represented by eq 1 was not included. Preliminary modeling indicated that a significant quantity of such replacements resulted in flatter simulated titration curves below the pH_{znpc}, which mimicked the higher temperature 0.03 *m* NaCl(Tr) data (Figure 3 right) but not the corresponding RbCl titrations (Figure 3 left), which showed no such flattening. Moreover, establishing definitive titration data trends below the pH_{znpc} was not possible because the accessible pH range is narrow and the "missing" proton concentration is small relative to the free proton concentration in these acidic solutions. Therefore, the replacement reaction was not incorporated into the final SCM.

A more subtle CMD adsorption trend was the inward movement of Rb^+ and Na^+ with increasing negative charge, even when bound in the same adsorption configuration. This is illustrated in Figure 5 for Rb^+ (top) and Na^+ (bottom) and results from increased Coulombic attraction. Between −0.1 and −0.2 C/m^2, the movement inward amounts to about 0.1 Å, which, although slight, is not accounted for in the present or any other SCM. A potential incorporation strategy would be to formulate charge-dependent CD and/or C_S terms, but how to do that while the relative simplicity of SCMs is also maintained is not yet apparent. It should be noted that such a charge-dependent CD or C_S SCM would be distinct from the variable capacitance model (VCM) recently proposed by Boily,[42] in which interfacial capacitance values are crystal face specific.

The inward movement of Rb^+ due to increased Coulombic attraction may also explain the 0.28 Å height increase for Rb^+ in TD coordination in going from the XR results of Zhang et al.[34] to the RAXR results of Kohli et al.[39] The former study was conducted in 1 *m* RbCl at pH 12 and the latter in 0.001 M RbOH at pH 11, and extrapolating our SCM for Rb^+ to those conditions results in estimated surface charges of −0.39 and −0.16 C/m^2, respectively. Consequently, the lower negative charge in the Kohli et al.[39] study and the resulting decreased Coulombic attraction may at least be partly responsible for the higher Rb^+ adsorption height (3.72 vs 3.44 Å) they reported [39]

5. SUMMARY AND FUTURE DIRECTIONS

The CD-MUSIC SCMs we have formulated for the RbCl−rutile and combined NaCl−NaTr−rutile systems are the most molecularly consistent SCMs yet available over a wide range of temperature, pH, and ionic strength. Our ability to quantitatively constrain CD-MUSIC was more successful for

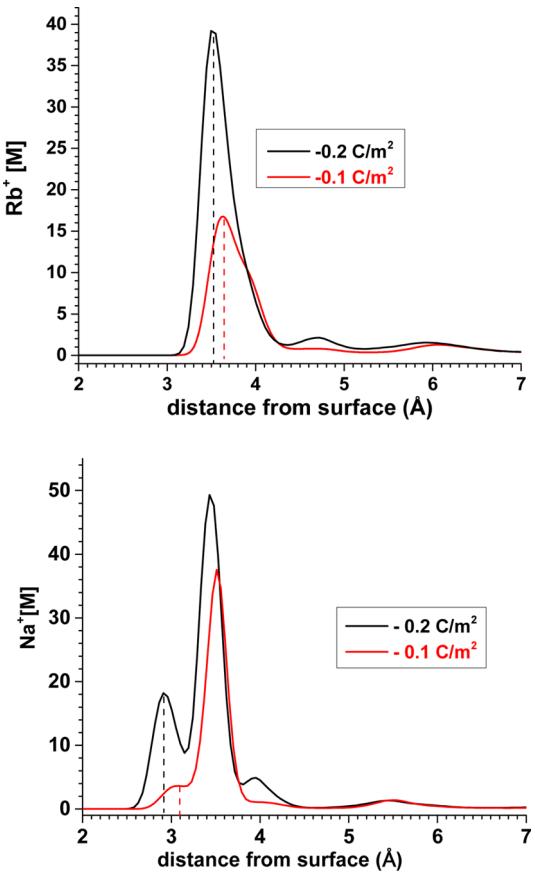

Figure 5. Axial density profiles at 25 °C for Rb^+ (top) and Na^+ (bottom) at −0.1 (red line) and −0.2 C/m^2 (black line). The vertical dotted lines indicate the approximate peak distances [above the (110) surface plane] at the inner-sphere tetradentate site.

RbCl than for NaCl(Tr) media. This was because Rb^+ binding is predominately tetradentate under all negative charge conditions and temperatures, which meant that only the tetradentate binding constant required significant adjustment in order to reflect the dominance of that site, while also providing a good fit to the corresponding titration data. In NaCl media, however, two types of bidentate binding, in addition to tetradentate binding, were significant at lower negative charge and temperatures. Despite numerous adjustments to the corresponding tetradentate and bidentate binding constants, we were not able to achieve a close match between the constrained CD-MUSIC fits to the titration data and the bidentate/tetradentate binding site ratios for Na^+ observed via CMD at both negative charge conditions (−0.2 and −0.1 C/m^2). Consequently, we settled for a good match at −0.2 C/m^2.

The CMD results also revealed that adsorbed Rb^+ and Na^+ were drawn closer to the rutile (110) surface with increasing negative charge even when bound in the same adsorption configuration (e.g., tetradentate). Although this movement is not captured in CD-MUSIC (or any other SCM) it could be mimicked by incorporating Stern-layer capacitance or CD values that vary with charge in future versions of the model. Moreover, since the CD and Stern-layer capacitance values that govern the electrostatic component of CD-MUSIC are based on mean field electrostatics, it is possible that more sophisticated potential of mean force electrostatic approaches will yield more robust SCMs.[43] Future SCMs must utilize more realistic molecular modeling inputs that incorporate dissociable

DOI: 10.1021/acs.jpcc.5b02841
J. Phys. Chem. C XXXX, XXX, XXX−XXX

water as well as water and ion polarizability. Additionally, the models need to be applied to a variety of mineral−water interfaces over a range of physical−chemical conditions. These interfaces should include those bounded by well-defined crystal faces and various aqueous solution compositions, which, when characterized by a wide variety of experimental techniques including surface charge and ion adsorption experiments, will provide corresponding macroscopic data for developing ever more realistic SCMs.

■ ASSOCIATED CONTENT

Supporting Information

An Excel file containing the rutile powder titration data and model fits discussed; the first worksheet contains the data and model fits for the RbCl media titrations, and the second worksheet contains the data and model fits for the NaCl(Tr) media titrations. The Supporting Information is available free of charge on the ACS Publications website at DOI: 10.1021/acs.jpcc.5b02841.

■ AUTHOR INFORMATION

Corresponding Author

*E-mail: machesky@illinois.edu. Tel: 217-222-9322.

Notes

The authors declare no competing financial interest.

■ ACKNOWLEDGMENTS

M.L.M. and D.J.W. were supported by the Division of Chemical Sciences, Geoscience and Biosciences, Office of Basic Energy Sciences, U.S. Department of Energy. M.K.R. acknowledges the support of the National Science Foundation (EAR-0842526). M.P. was supported by the Czech Science Foundation (13-08651S). The comments of two anonymous reviewers were greatly appreciated and resulted in an improved final manuscript.

■ REFERENCES

(1) Brown, G. E., Jr.; Calas, G. Mineral−Aqueous Solution Interfaces and Their Impact on the Environment. *Geochem. Perspect.* **2012**, *1*, 483−742.

(2) Dzombak, D. A.; Morel, F. M. M. *Surface Complexation Modeling: Hydrous Ferric Oxide*; John Wiley and Sons: New York, 1990; p 393.

(3) Lützenkirchen, J. *Surface Complexation Modelling*; Elsevier: New York, 2006; p 638.

(4) Stumm, W.; Hohl, H.; Dalang, F. Interaction of Metal Ions with Hydrous Oxide Surfaces. *Croat. Chem. Acta* **1976**, *48*, 491−504.

(5) Schindler, P. W.; Fürst, B.; Dick, R.; Wolf, P. U. Ligand Properties of Surface Silanol Groups. I. Surface Complex Formation with Fe^{3+}, Cu^{2+}, Cd^{2+}, and Pb^{2+}. *J. Colloid Interface Sci.* **1976**, *55*, 469−475.

(6) Yates, D. E.; Levine, S.; Healy, T. W. Site-Binding Model of the Electrical Double Layer at the Oxide/Water Interface. *J. Chem. Soc., Faraday Trans. 1* **1974**, *70*, 1807−1818.

(7) Davis, J. A.; James, R. O.; Leckie, J. O. Surface Ionization and Complexation at the Oxide/Water Interface: I. Computation of Electrical Double Layer Properties in Simple Electrolytes. *J. Colloid Interface Sci.* **1978**, *63*, 480−499.

(8) Westall, J.; Hohl, H. A Comparison of Electrostatic Models for the Oxide/Solution Interface. *Adv. Colloid Interface Sci.* **1980**, *12*, 265−294.

(9) Tejedor-Tejedor, M. I.; Anderson, M. A. "In Situ" ATR-Fourier Transform Infrared Studies of the Goethite (α-FeOOH)−Aqueous Solution Interface. *Langmuir* **1986**, *2*, 203−210.

(10) Hayes, K. F.; Roe, A. L.; Brown, G. E., Jr.; Hodgson, K. O.; Leckie, J. O.; Parks, G. A. In Situ X-ray Absorption Study of Surface Complexes: Selenium Oxyanions on Goethite (α-FeOOH). *Science* **1987**, *238*, 783−786.

(11) Rustad, J. R.; Felmy, A. R.; Hay, B. P. Molecular Statics Calculations for Iron Oxide and Oxyhydroxide Minerals: Toward a Flexible Model of the Reactive Mineral−Water Interface. *Geochim. Cosmochim. Acta* **1996**, *60*, 1553−1562.

(12) Wasserman, E.; Rustad, J. R.; Felmy, A. R.; Hay, B. P.; Halley, J. W. Ewald Methods for Polarizable Surfaces with Application to Hydroxylation and Hydrogen Bonding on the (012) and (001) Surfaces of α-Fe_2O_3. *Surf. Sci.* **1997**, *385*, 217−239.

(13) Sverjensky, D. A.; Fukushi, K. Anion Adsorption on Oxide Surfaces: Inclusion of the Water Dipole in Modeling the Electrostatics of Ligand Exchange. *Environ. Sci. Technol.* **2006**, *40*, 263−271.

(14) Hiemstra, T.; Venema, P.; VanRiemsdijk, W. H. Intrinsic Proton Affinity of Reactive Surface Groups of Metal (Hydr)Oxides: The Bond Valence Principle. *J. Colloid Interface Sci.* **1996**, *184*, 680−692.

(15) Hiemstra, T.; VanRiemsdijk, W. H. A Surface Structural Approach to Ion Adsorption: The Charge Distribution (CD) Model. *J. Colloid Interface Sci.* **1996**, *179*, 488−508.

(16) Hiemstra, T.; Van Riemsdijk, W. H. On the Relationship between Charge Distribution, Surface Hydration, and the Structure of the Interface of Metal Hydroxides. *J. Colloid Interface Sci.* **2006**, *301*, 1−18.

(17) Ridley, M. K.; Hiemstra, T.; van Riemsdijk, W. H.; Machesky, M. L. Inner-Sphere Complexation of Cations at the Rutile−Water Interface: A Concise Surface Structural Interpretation with the CD and MUSIC Model. *Geochim. Cosmochim. Acta* **2009**, *73*, 1841−1856.

(18) Předota, M.; Bandura, A. V.; Cummings, P. T.; Kubicki, J. D.; Wesolowski, D. J.; Chialvo, A. A.; Machesky, M. L. Electric Double Layer at the Rutile (110) Surface. 1. Structure of Surfaces and Interfacial Water from Molecular Dynamics by Use of Ab Initio Potentials. *J. Phys. Chem. B* **2004**, *108*, 12049−12060.

(19) Předota, M.; Zhang, Z.; Fenter, P.; Wesolowski, D. J.; Cummings, P. T. Electric Double Layer at the Rutile (110) Surface. 2. Adsorption of Ions from Molecular Dynamics and X-ray Experiments. *J. Phys. Chem. B* **2004**, *108*, 12061−12072.

(20) Předota, M.; Vlcek, L. Comment on Parts 1 and 2 of the Series "Electric Double Layer at the Rutile (110) Surface". *J. Phys. Chem. B* **2007**, *111*, 1245−1247.

(21) Předota, M.; Machesky, M. L.; Wesolowski, D. J.; Cummings, P. T. Electric Double Layer at the Rutile (110) Surface. 4. Effect of Temperature and pH on the Adsorption and Dynamics of Ions. *J. Phys. Chem. C* **2013**, *117*, 22852−22866.

(22) Matsui, M.; Akaogi, M. Molecular Dynamics Simulation of the Structural and Physical Properties of the Four Polymorphs of TiO_2. *Mol. Simul.* **1991**, *6*, 239−244.

(23) Machesky, M. L.; Wesolowski, D. J.; Palmer, D. A.; Ichiro-Hayashi, K. Potentiometric Titrations of Rutile Suspensions to 250 °C. *J. Colloid Interface Sci.* **1998**, *200*, 298−309.

(24) Ridley, M. K.; Machesky, M. L.; Palmer, D. A.; Wesolowski, D. J. Potentiometric Studies of the Rutile−Water Interface: Hydrogen-Electrode Concentration-Cell Versus Glass-Electrode Titrations. *Colloids Surf., A* **2002**, *204*, 295−308.

(25) Machesky, M. L.; Wesolowski, D. J.; Palmer, D. A.; Ridley, M. K.; Benezeth, P.; Lvov, S. N.; Fedkin, M. V., Ion Adsorption into the Hydrothermal Regime: Experimental and Modeling Approaches. In *Surface Complexation Modelling*; Johannes, L., Ed.; Elsevier: New York, 2006; pp 324−358.

(26) Bourikas, K.; Hiemstra, T.; Van Riemsdijk, W. H. Ion Pair Formation and Primary Charging Behavior of Titanium Oxide (Anatase and Rutile). *Langmuir* **2001**, *17*, 749−756.

(27) Livi, K. J. T.; Schaffer, B.; Azzolini, D.; Seabourne, C. R.; Hardcastle, T. P.; Scott, A. J.; Hazen, R. M.; Erlebacher, J. D.; Brydson, R.; Sverjensky, D. A. Atomic-Scale Surface Roughness of Rutile and Implications for Organic Molecule Adsorption. *Langmuir* **2013**, *29*, 6876−6883.

(28) Machesky, M. L.; Predota, M.; Wesolowski, D. J.; Vlcek, L.; Cummings, P. T.; Rosenqvist, J.; Ridley, M. K.; Kubicki, J. D.; Bandura, A. V.; Kumar, N.; Sofo, J. O. Surface Protonation at the

DOI: 10.1021/acs.jpcc.5b02841
J. Phys. Chem. C XXXX, XXX, XXX−XXX

Rutile (110) Interface: Explicit Incorporation of Solvation Structure within the Refined Music Model Framework. *Langmuir* **2008**, *24*, 12331−12339.
(29) Kumar, N.; Kent, P. R. C.; Bandura, A. V.; Kubicki, J. D.; Wesolowski, D. J.; Cole, D. R.; Sofo, J. O. Faster Proton Transfer Dynamics of Water on SnO_2 Compared to TiO_2. *J. Chem. Phys.* **2011**, *134*, 0447061−0447067.
(30) Kumar, N.; Kent, P. R. C.; Wesolowski, D. J.; Kubicki, J. D. Modeling Water Adsorption on Rutile (110) Using van der Waals Density Functional and Dft+U Methods. *J. Phys. Chem. C* **2013**, *117*, 23638−23644.
(31) Raju, M.; Kim, S.-Y.; van Duin, A. C. T.; Fichthorn, K. A. Reaxff Reactive Force Field Study of the Dissociation of Water on Titania Surfaces. *J. Phys. Chem. C* **2013**, *117*, 10558−10572.
(32) Huang, L.; Gubbins, K. E.; Li, L.; Lu, X. Water on Titanium Dioxide Surface: A Revisiting by Reactive Molecular Dynamics Simulations. *Langmuir* **2014**, *30*, 14832−14840.
(33) Bandura, A. V.; Kubicki, J. D.; Sofo, J. O. Comparisons of Multilayer H_2O Adsorption onto the (110) Surfaces of α-TiO_2 and SnO_2 As Calculated with Density Functional Theory. *J. Phys. Chem. B* **2008**, *112*, 11616−11624.
(34) Zhang, Z.; Fenter, P.; Sturchio, N. C.; Bedzyk, M. J.; Machesky, M. L.; Wesolowski, D. J. Structure of Rutile TiO_2 (110) in Water and 1 Molal Rb^+ at pH 12: Inter-Relationship among Surface Charge, Interfacial Hydration Structure, and Substrate Structural Displacements. *Surf. Sci.* **2007**, *601*, 1129−1143.
(35) Machesky, M. L.; Wesolowski, D. J.; Palmer, D. A.; Ridley, M. K. On the Temperature Dependence of Intrinsic Surface Protonation Equilibrium Constants: An Extension of the Revised Music Model. *J. Colloid Interface Sci.* **2001**, *239*, 314−327.
(36) Ridley, M. K.; Machesky, M. L.; Wesolowski, D. J.; Palmer, D. A. Modeling the Surface Complexation of Calcium at the Rutile−Water Interface to 250°C. *Geochim. Cosmochim. Acta* **2004**, *68*, 239−251.
(37) Driesner, T.; Seward, T. M.; Tironi, I. G. Molecular Dynamics Simulation Study of Ionic Hydration and Ion Association in Dilute and 1 Molal Aqueous Sodium Chloride Solutions from Ambient to Supercritical Conditions. *Geochim. Cosmochim. Acta* **1998**, *62*, 3095−3107.
(38) Fulton, J. L.; Pfund, D. M.; Wallen, S. L.; Newville, M.; Stern, E. A.; Ma, Y. Rubidium Ion Hydration in Ambient and Supercritical Water. *J. Chem. Phys.* **1996**, *105*, 2161.
(39) Kohli, V.; Zhang, Z.; Park, C.; Fenter, P. Rb^+ and Sr^{2+} Adsorption at the TiO_2(110)−Electrolyte Interface Observed with Resonant Anomalous X-ray Reflectivity. *Langmuir* **2009**, *26*, 950−958.
(40) Parez, S.; Předota, M.; Machesky, M. Dielectric Properties of Water at Rutile and Graphite Surfaces: Effect of Molecular Structure. *J. Phys. Chem. C* **2014**, *118*, 4818−4834.
(41) Cheng, J.; Sprik, M. The Electric Double Layer at a Rutile TiO_2 Water Interface Modelled Using Density Functional Theory Based Molecular Dynamics Simulation. *J. Phys.: Condens. Matter* **2014**, *26*, 244108.
(42) Boily, J.-F. The Variable Capacitance Model: A Strategy for Treating Contrasting Charge-Neutralizing Capabilities of Counterions at the Mineral/Water Interface. *Langmuir* **2014**, *30*, 2009−2018.
(43) Attard, P. Fits to Hypernetted Chain Calculations for Electrostatic Potential and Ion Concentrations for Use in Surface Complexation. In *Surface Complexation Modelling*; Lutzenkirchen, J., Ed.; Elsevier: New York, 2006; pp 88−111.

DOI: 10.1021/acs.jpcc.5b02841
J. Phys. Chem. C XXXX, XXX, XXX−XXX